Available online at www.sciencedirect.com
ScienceDirect
Journal of Power Sources 179 (2008) 649–659
JOURNAL OF POWER SOURCES
www.elsevier.com/locate/jpowsour

Adaptive control of the airflow of a PEM fuel cell system

Junzhi Zhang [a], Guidong Liu [a,*], Wensheng Yu [b], Minggao Ouyang [a]

[a] State Key Laboratory of Automotive Safety and Energy, Tsinghua University, Beijing 100084, PR China
[b] Key Lab of Complex Systems and Intelligence Science, Chinese Academy of Sciences, Beijing 100080, PR China

Received 23 December 2007; accepted 7 January 2008
Available online 16 January 2008

Abstract

An appropriate oxygen excess ratio could improve the net power of a fuel cell system and reduce the potential of oxygen starvation. Due to nonlinear and time-varying characteristics, it is a difficult task to maintain the oxygen excess ratio within an ideal range particularly during transients. An adaptive control algorithm is therefore proposed to dynamically stabilize the oxygen excess ratio around an optimal level. The application of the algorithm inevitably involves the estimation of time-varying parameters and the pole assignment of the closed-loop system. The proposed adaptive control is evaluated on a test bench, and its application to overcome the time-varying problem is demonstrated.
© 2008 Elsevier B.V. All rights reserved.

Keywords: Fuel cell; Air-supply subsystem; Adaptive control; Estimation

1. Introduction

Stimulated by attempts to overcome energy shortages and alleviate pollution caused by emissions from energy consumption, many countries devote great effort to exploring and making use of new energy resources. Because proton exchange membrane (PEM) fuel cells boast many ingenious features, such as high power density, fast startup, suitability for discontinuous operation, low noise, and environmental friendliness [1–4], they are now under intensive development by many governments, manufacturers, and researchers.

The air-supply subsystem is very important in a PEM fuel cell system [5]. Excess oxygen replenishment into the cathode will cause power waste, consequently leading to a decrease in the net power of the fuel cell system. Conversely, if fuel cells are subject to oxygen starvation, the potential of these cells will suffer from deterioration. If the starvation is not too serious and the oxygen is enough to maintain the stack current, the voltage of the fuel cells is positive. However, if fluxes of oxygen are not enough to maintain the stack current, there must be an electrolysis current that makes the voltage of the starved cells drop to negative-named "cell reversal" [6]. In this case, the protons transported from the anode will be oxidized in the cathode to form hydrogen and the cell essentially acts as a hydrogen pump [7]. The electrode half reactions and the overall reaction are as below:

$$\begin{aligned} &\text{anode}: \quad H_2(a) \rightarrow 2H^+ + 2e^- \\ &\text{cathode}: \quad 2H^+ + 2e^- \rightarrow H_2(c) \\ &\text{overall}: \quad H_2(a) \rightarrow H_2(c) \end{aligned} \tag{1}$$

While the process of air replenishment is directly related to oxygen starvation [8–10], many researchers have been focusing on the air-supply kinetics in the past decade. Vahidi et al. [11] investigated oxygen starvation in a fuel cell/super-capacitor hybrid system. The proposed model-predicting controller can avoid the oxygen starvation phenomenon despite load fluctuations. Pukrushpan [12] designed a model-based air-supply controller, which could optimize the air-supply subsystem in principle but this lacks experimental support. Methekar et al. [13] presented a distributed PEM fuel cell model and studied its dynamics. Subsequently, a proportional control strategy has been attempted to reduce oxygen starvation. Feroldi et al. [14] proposed a coordinative control strategy that regulates the airflow replenished into the system and the exhaust exiting the system simultaneously. As a result, both the oxygen excess ratio and fuel cell voltage are well under control. However, the effectiveness of the proposed strategy has not been verified with experiments thus far. Rodatz et al. [15] developed a dynamic model of an air-supply subsystem as well as a linear

* Corresponding author. Tel.: +86 01 62771839.
E-mail address: public1976@163.com (G. Liu).

0378-7753/$ – see front matter © 2008 Elsevier B.V. All rights reserved.
doi:10.1016/j.jpowsour.2008.01.015

Nomenclature

A	area (cm^2)
ca	cathode of fuel cell stack
e^-	minus electron
ex	expectation
f	gas flow ($mol\ s^{-1}$)
F	Faraday Constant
gfr	gas flow regulator
H^+	proton
H_2	hydrogen
i	current (A)
N	number of cells
N_2	nitrogen
O_2	oxygen
p	pressure (kPa)
R	universal gas constant ($8.3143\ J\ K\ mol^{-1}$)
u	voltage (V)
V	volume (L)
τ	time constant (s)

quadratic regulator for a PEM fuel cell system. According to the results presented in this paper, the improvement in performance achieved by this controller was noticeable. Moreover, the pressure control is successfully decoupled from the mass flow control, resulting in a fast response. Pukrushpan et al. [16,17] presented a single-input single-output (SISO) linear state feedback controller for the air stoichiometric ratio. Although a semi-empirical fuel cell model was used, it does provide an insight into the transient behavior of the air-supply subsystem. Caux et al. [18] studied an approach to control the air-supply subsystem which is particularly effective during transients. A specific balance model is used to maintain a constant pressure on the cathode compartment and to follow a desired airflow rate.

The complex, time-varying and nonlinear dynamics of the air-supply subsystem is usually approximated by the principle of mass conservation, theories of fluid kinetics, thermodynamics and heat transfer under various assumptions and constraints. Popularly applied models all inaccurately describe the dynamics, and the accuracies of the approximations vary with the shift of operating points. This problem has attracted much attention. Yang et al. [19] proposed a systematic method of identification and control of a PEM fuel cell. Supported by simulation results, an adaptive controller has proven to be robust despite the variation in parameters and the presence of disturbances. Golbert and Lewin [20] developed a time-varying state space model, analyzed its controllability, and presented a nonlinear adaptive controller. These adaptive strategies indicate a trend that future attempts to develop nonlinear models must oversee the entire operating range to optimize the stable and dynamic performance of fuel cell systems.

As shown in previous literature, air-supply subsystems exhibit time-varying and nonlinear properties. This inevitably poses a difficulty in accurate and dynamic regulation of air replenishment. While most works focusing on these problems were presented with simulation results, this paper presents experimental validations of an adaptive strategy.

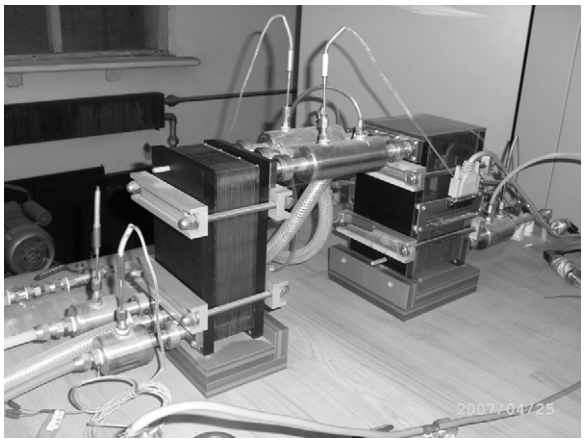

Fig. 1. Fuel cell system.

The remainder of this paper is arranged as follows. The kinetics of an air-supply subsystem and its time-varying and nonlinear property are introduced in Section 2, followed by a design of the adaptive control strategy to achieve an optimal oxygen excess ratio in Section 3. After discussing the experimental results in Section 4, conclusions are presented in Section 5.

2. Dynamics of air-supply subsystem

This paper examines a membrane-humidifying PEM fuel cell, as shown in Fig. 1, with an active cell area of 150 cm^2, 24 Nafion112 cells in series, and 1 kW gross power, operating temperature of 65 ° C and pressure in the stack of 30 kPa. Fig. 2 shows the structure of our fuel cell system. There are four major control subsystem loops that adjust the air/hydrogen supply, the humidity of reactants, the temperature in stack, and the power output [21].

Membrane humidifying is accepted as an excellent mechanism for PEM fuel cells [22,23]. In this configuration, the thin humidifying membrane (thickness of 0.051–0.183 mm) makes it possible for gas flow to have sufficient contact with the saturated vapor, thus humidifying is efficient [24]. Therefore, we assume here a perfect air/hydrogen flow humidifier. In addition, a cooler is applied to regulate the excess heat generated during reactions. Due to the fast dynamics of the cooler, the temperature of the stack can be controlled to be within a proper range. Moreover, a fast proportional controller of the fuel flow ensures

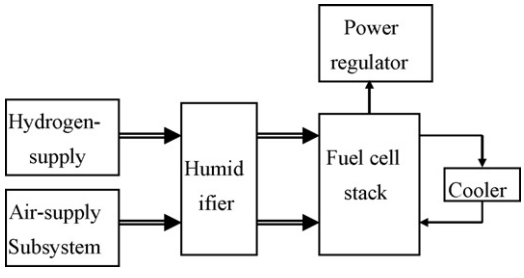

Fig. 2. Scheme of fuel cell stack.

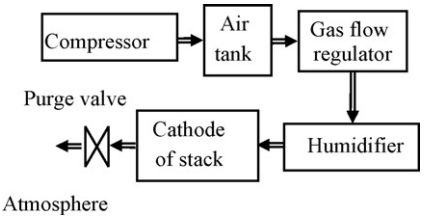

Fig. 3. Scheme of air-supply system.

the pressure in anode compartment tracks that in the cathode compartment almost instantaneously. All these controllers and assumptions are by no means trivial but make the concentration of this paper on the control of the air-supply subsystem possible.

As shown in Fig. 3, the air-supply system mainly consists of a compressor driven by an electric motor, an air tank for compressed air reservation, an gas flow regulator to dynamically regulate the replenishment of air into the cathode, and the volume of the cathode manifold that houses the air-supply pipes, cathode, cooler and humidifier. Additionally, the air has to be humidified to prevent drying-out of the membrane of the fuel cells.

2.1. Modelling of the airflow channel

Before modelling the air-supply subsystem, several assumptions and simplifications are introduced, so we can focus on the transient behavior of air replenishment: (1) all gases obey the ideal gas law due to the low operating pressure (with respective to the atmospheric pressure); (2) as the volume of the stack is relatively small and the coolant can sufficiently carry the heat generated in the process of the reaction, the temperature of the air inside the cathode equals to the bulk stack temperature that is, in turn, equal to the temperature of the coolant exiting the stack; (3) the properties of the gas flow exiting the cathode such as temperature and pressure are assumed to be the same as those inside the cathode and they dominate the reaction in the catalyst layers in the membrane; (4) because the humidifier is effective as explained previously, the gas in the cathode is almost fully humidified and the liquid water generated inside the cathode is no longer vaporized; (5) any extra water inside the cathode could be carried out with the exhaust gas; (6) the flow channel and gas diffusion layer are lumped into one volume, i.e. the spatial variations are neglected; and (7) the gas pressure in the air tank can be kept constant on the assumption that air could be replenished into the air tank by the compressor under the regulation of an independent controller.

The mass continuity of the oxygen and nitrogen inside the cathode volume and ideal gas law yields:

$$\frac{\mathrm{d}p_{\mathrm{O_2,ca}}}{\mathrm{d}t} = \frac{RT_{\mathrm{ca}}}{V_{\mathrm{ca}}}(f_{\mathrm{O_2,gfr}} - f_{\mathrm{O_2,used}} - f_{\mathrm{O_2,ca,out}}) \tag{2}$$

$$\frac{\mathrm{d}p_{\mathrm{N_2,ca}}}{\mathrm{d}t} = \frac{RT_{\mathrm{ca}}}{V_{\mathrm{ca}}}(f_{\mathrm{N_2,gfr}} - f_{\mathrm{N_2,ca,out}}) \tag{3}$$

where d is the differential operator; $f_{\mathrm{O_2,used}}$, $f_{\mathrm{O_2,ca,out}}$ and $f_{\mathrm{N_2,ca,out}}$ are mole flow rate of O_2 used in reaction, mole flow rates of O_2 and N_2 in stack outlet, respectively.

Experiment results [25] showed the gas flow regulator is a typical nonlinear system, which, given the input and output signals, can be approximated by linear models at various operating points as

$$\tau_{\mathrm{gfr}}\frac{\mathrm{d}f_{\mathrm{air,gfr}}}{\mathrm{d}t} = -f_{\mathrm{air,gfr}} + k_{wf}K_{\mathrm{gfr}}u_{\mathrm{gfr}} \tag{4}$$

$$f_{\mathrm{O_2,gfr}} = 0.21\, f_{\mathrm{air,gfr}} \tag{5}$$

$$f_{\mathrm{N_2,gfr}} = 0.79\, f_{\mathrm{air,gfr}} \tag{6}$$

where $k_{wf} = 1/(22.4 \times 60)$ mol (L s)$^{-1}$ and K_{gfr} is the gain of the gas flow regulator.

Eq. (2)–(6) consist of the model of the air-supply subsystem.

2.2. Analysis of the property of the gas flow regulator

As the gas flow regulator shown in Fig. 4 is a component that replenishes air into the stack cathode, its dynamics are critical to the air-supply subsystem. The gas flow regulator is a complex of mechanics and electronics. Its inputs, outputs and parameters are subject to the variations in the inner and outer environments such as electromagnetism, temperature, humidity and gas pressure at the outlet. What is more, there is an obvious nonlinear property in some operating regions especially at a small command voltage and this property has distinct influence on the dynamics of airflow, which, from control point of view, can be treated as a time-varying property at different operating points. For these reasons, investigations were carried out to identify the disturbance and time-varying property of the gas flow regulator.

Many tests [25] yielded an experimental model of the gas flow regulator at a certain operating point according to Eq. (4):

$$\tau_{\mathrm{gfr}}\frac{\mathrm{d}f_{\mathrm{air,gfr}}}{\mathrm{d}t} = -f_{\mathrm{air,gfr}} + k_{wf}K_{\mathrm{gfr}}u_{\mathrm{gfr}} + \nabla f_{\mathrm{air,gfr}} + k_{wf}K_{\mathrm{gfr}}\nabla u_{\mathrm{gfr}} \tag{7}$$

where $\nabla f_{\mathrm{air,gfr}}$ and ∇u_{gfr} are disturbances and higher-order dynamics of $f_{\mathrm{air,gfr}}$ and u_{gfr}, respectively. Experimental data [25] showed that $\nabla f_{\mathrm{air,gfr}}$ and ∇u_{gfr} both have Gaussian distributions with zero means to some extent. Because they are independent of one another, their summation still has a Gaussian distribution as shown in

$$\epsilon = \nabla f_{\mathrm{air,gfr}} + k_{wf}K_{\mathrm{gfr}}\nabla u_{\mathrm{gfr}} \quad \epsilon \sim (0, \sigma^2_{\mathrm{gfr}}) \tag{8}$$

Substituting Eq. (8) into Eq. (7), a simplified model of the gas flow regulator is obtained as

$$\tau_{\mathrm{gfr}}\frac{\mathrm{d}f_{\mathrm{air,gfr}}}{\mathrm{d}t} = -f_{\mathrm{air,gfr}} + k_{wf}K_{\mathrm{gfr}}u_{\mathrm{gfr}} + \epsilon \tag{9}$$

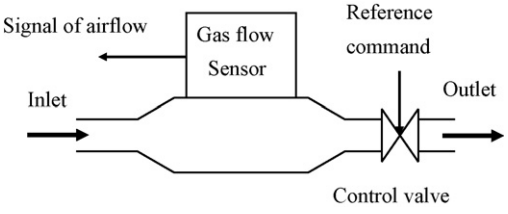

Fig. 4. Scheme of gas flow regulator.

Thus far, Eq. (4) can be modified as Eq. (9) in consideration of disturbances and higher-order dynamics of $f_{\text{air,gfr}}$ and u_{gfr}.

To investigate the time-varying property of the gas flow regulator, tests are carried out to identify the parameters of the gas flow regulator at various operating points.

For convenient analysis of the time-varying property by parameter identification, the linear system model Eq. (9) is represented as a discrete-time equation of the difference operator, and this leads to an auto-regressive moving-average with an auxiliary input model, the ARMAX model [26]:

$$\begin{cases} A_{\text{gfr}}(z^{-1}) f_{\text{air,gfr}}(k) = B_{\text{gfr}}(z^{-1}) u_{\text{gfr}}(k) + \epsilon(k) \\ A_{\text{gfr}}(z^{-1}) = 1 + a_1 z^{-1} + a_2 z^{-2} + \cdots + a_r z^{-r} \\ B_{\text{gfr}}(z^{-1}) = b_1 z^{-1} + b_2 z^{-2} + \cdots + b_r z^{-r} \end{cases} \tag{10}$$

where integer k denotes the time instant of sampling and r is the system order. In a succinct form, the term $A_{\text{gfr}}(z^{-1}) f_{\text{air,gfr}}(k)$ is the auto-regression part, where z^{-1} is a backward shift operator, and $z^{-h} f_{\text{air,gfr}}(k)$ represents the past output $f_{\text{air,gfr}}(k-h)$, $h = 1, 2, \ldots, r$; $B_{\text{gfr}}(z^{-1}) u_{am}(k)$ denotes the moving average of the past inputs, where $z^{-h} u_{am}(k) = u_{am}(k-h)$, $h = 1, 2, \ldots, r$; and the auxiliary input $\epsilon(k)$ is included to better describe the unmodelled dynamics of the system, including higher-order dynamics and disturbances. Therefore, the corresponding transfer function between output and input in the discrete-time form becomes

$$G_{\text{gfr}} = \frac{B_{\text{gfr}}(z)}{A_{\text{gfr}}(z)} \tag{11}$$

According to the theory of parameter identification, all system modes can be excited by a white noise, whose frequency contents consist entirely of sinusoidal waves of the same amplitude or strength. In the real world, a signal with a rich content of frequencies can be generated by an M-series, and this signal approximately satisfies the persistent excitation requirement for system identification.

In the process of identification, the model of the gas flow regulator is regarded as a black box, as shown in Fig. 5. The reference command, $u_{\text{gfr}}(k)$, is an M-series with mean value at the operating point, and $f_{\text{air,gfr}}(k)$ is the airflow response at the excitation of $u_{\text{gfr}}(k)$. $G_{\text{gfr}}(z^{-1})$ mathematically represents the dynamics of the gas flow regulator. $\epsilon(k)$ stands for the noise arising from the inner and outer environments, and other disturbances.

For convenience of identification, Eq. (10) is rewritten as

$$f_{\text{air,gfr}}(k) = h_{\text{gfr}}(k)\theta_{\text{gfr}} + \epsilon(k) \tag{12}$$

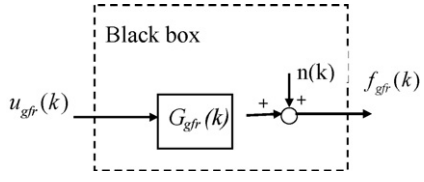

Fig. 5. Blackbox for parameter identification.

where

$$\begin{cases} h_{\text{gfr}} = [-f_{\text{air,gfr}}(i-1), \cdots, -f_{\text{air,gfr}}(i-r), \\ \qquad u_{\text{gfr}}(i-1), \ldots, u_{\text{gfr}}(i-r)]^T \\ \theta_{\text{gfr}} = [a_1, a_2, \ldots, a_r, b_1, b_2, \ldots, b_r]^T \\ i = 1, 2, \ldots, L \\ L = 1200 \end{cases}$$

where T is the transposition operator.

In addition, the characteristic of the noise, $\epsilon(k)$, can be described by its first and second order moments, expressed as

$$E\{\overrightarrow{\epsilon}\} = [E\{\epsilon(1)\}, E\{\epsilon(2)\}, \cdots, E\{\epsilon(L)\}]^T \tag{13}$$

$$Cov\{\overrightarrow{\epsilon}\} = E\{\overrightarrow{\epsilon}\,\overrightarrow{\epsilon}^T\} = \begin{bmatrix} E\{\epsilon^2(1)\} & E\{\epsilon(1)\epsilon(2)\} & \cdots & E\{\epsilon(1)\epsilon(L)\} \\ E\{\epsilon(2)\epsilon(1)\} & E\{\epsilon^2(2)\} & \cdots & E\{\epsilon(2)\epsilon(L)\} \\ E\{\epsilon(3)\epsilon(1)\} & E\{\epsilon(3)\epsilon(2)\} & \cdots & E\{\epsilon(3)\epsilon(L)\} \\ \cdots & \cdots & \cdots & \cdots \\ E\{\epsilon(L)\epsilon(1)\} & E\{\epsilon(L)\epsilon(2)\} & \cdots & E\{\epsilon^2(L)\} \end{bmatrix} \tag{14}$$

where $E\{\,\}$ is the expected value operator and Cov is the correlation operator.

The criterion function can be adopted as

$$J_{\text{gfr}}(\theta_{\text{gfr}}) = \sum_{k=1}^{L} [f_{\text{air,gfr}}(k) - h_{\text{gfr}}(k)\theta_{\text{gfr}}]^2 \tag{15}$$

Minimizing $J_{\text{gfr}}(\theta_{\text{gfr}})$ gives the estimation of θ_{gfr}.

The parameters of the gas flow regulator used in the experiment are: a main time constant, about 2 s; a frequency band, 30 Hz; an airflow range, 0–100 L min^{-1} responding to the reference command, 0–5 V. The characteristic polynomial of the M-series is adopted as

$$F(s) = s^{10} \otimes s^9 \otimes s^4 \otimes s \otimes 1 \tag{16}$$

and the period of the impulse is $(1/60)s$; the test time is 20 s and the datum length is 1200. The normalized M-series used in the test process is illustrated in Fig. 6. Before the test begins, the compressor is run under its controller to replenish air into the air tank until the pressure reaches 200 kPa. In the process of the test, the opening extent of the purge valve (OTPV) is divided into six levels, and at each level, M-series voltages are exerted on the gas flow regulator as the reference command with mean values of 1 V, 1.5 V, 2 V, 2.5 V, 3 V and 3.5 V.[1] For each test state,[2] two tests are performed, and the input signals (M-series) and output signals (airflow from the gas flow regulator) are recorded simultaneously for further analysis.

The test data are analyzed by minimizing the criterion function Eq. (15), and the identified model is transformed into the continuous model that has the form of Eq. (9) with the parameters of K_{gfr} and τ_{gfr} shown in Tables 1 and 2.

[1] These voltages are typical operating points in the gas flow regulator.

[2] Test state is defined as the cross-point of each level of OTPV and each level of reference command voltage.

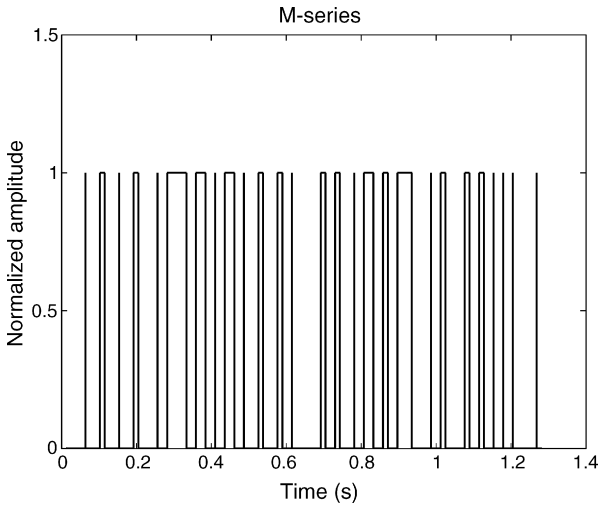

Fig. 6. M-series.

Note: The symbol, ∗, means the test is not run to prevent the gas flow regulator from risking excess pressure.

From Table 1, the reference commands with mean values of 1 and 1.5 V correspond to K_{gfr} values no larger than 3 L (min V)$^{-1}$, which are obviously smaller than those for the other reference commands, which have values larger than 19 L (min V)$^{-1}$. Therefore, before the reference command reaches an opening value of about 1.9 V, the airflow is almost out operation. Similarly, the data in Table 2 also shows the difference between reference commands with mean values of 1 and 1.5 V and other reference commands. The average values of τ_{gfr} for reference commands with mean values of 1 and 1.5 V are almost half those of τ_{gfr} for other reference commands. This result demonstrates that the main time constant, τ_{am}, behaves discontinuously in the whole range of operation. In addition, K_{am} varies slightly on the condition that the reference command is larger than 2 V, being within the range of 19.40 to 20.40 L (min V)$^{-1}$. However, τ_{am} undergoes obvious variation with change in the reference command and OTPV. To fur-

Table 1
Estimation of K_{gfr}

		Reference command voltage on gas flow regulator					
		1.0 V	1.5 V	2.0 V	2.5 V	3.0 V	3.5 V
	T.S. (1.1)	1.18	0.89	19.81	*	*	*
	T.S. (1.2)	1.07	0.88	19.59	*	*	*
O	T.S. (2.1)	1.34	0.70	19.41	19.48	19.55	*
	T.S. (2.2)	1.42	0.81	19.46	19.56	19.54	*
T	T.S. (3.1)	1.51	0.81	20.31	19.65	19.99	19.74
	T.S. (3.2)	1.08	0.81	19.76	19.62	19.53	19.86
P	T.S. (4.1)	2.55	0.96	20.25	20.11	19.74	20.04
	T.S. (4.2)	1.52	1.00	20.56	20.11	20.68	21.06
V	T.S. (5.1)	1.40	0.77	20.56	20.44	21.08	20.21
	T.S. (5.2)	1.39	0.81	20.40	20.88	20.02	20.35
	T.S. (6.1)	1.29	0.89	20.51	20.58	20.57	20.20
	T.S. (6.2)	1.33	0.85	20.45	20.50	19.99	20.40

Table 2
Estimation of τ_{gfr}

		Reference command voltage on gas flow regulator					
		1.0 V	1.5 V	2.0 V	2.5 V	3.0 V	3.5 V
	T.S. (1.1)	0.78	0.87	1.51	*	*	*
	T.S. (1.2)	0.89	0.92	1.39	*	*	*
O	T.S. (2.1)	0.87	0.98	1.83	1.85	1.99	*
	T.S. (2.2)	0.80	0.98	1.64	1.80	1.73	*
T	T.S. (3.1)	0.85	1.09	1.96	2.06	1.86	2.36
	T.S. (3.2)	1.02	0.99	1.94	1.91	2.07	2.06
P	T.S. (4.1)	1.90	0.98	2.01	2.19	2.13	2.45
	T.S. (4.2)	1.25	0.99	1.88	2.14	2.30	2.18
V	T.S. (5.1)	1.00	0.99	2.24	2.06	2.44	2.38
	T.S. (5.2)	0.93	1.05	1.96	2.15	2.20	2.11
	T.S. (6.1)	0.98	0.84	1.93	2.20	2.34	2.57
	T.S. (6.2)	1.03	0.90	2.09	2.17	2.16	2.42

ther investigate the relationship between τ_{am} and the reference command and OTPV, the methodology of variance analysis is employed.

As the test conditions are almost same, the two results in each test state are proximately belong to a Gaussian distribution. For convenience of analysis, OTPV is defined as the factor $\mathcal{A}$, and the six OTPVs are defined as six levels, $\mathcal{A}_1$, $\mathcal{A}_2$, $\mathcal{A}_3$, $\mathcal{A}_4$, $\mathcal{A}_5$ and $\mathcal{A}_6$. Similarly, the mean value of the reference command voltage is defined as factor $\mathcal{B}$. Because the open voltage of the gas flow regulator is about 1.9 V, the for the voltages of 1.0 and 1.5 V are meaningless in analysis. Thus, the four valid results for the mean voltages of 2.0, 2.5, 3.0 and 3.5 V are divided into four levels: $\mathcal{B}_1$, $\mathcal{B}_2$, $\mathcal{B}_3$ and $\mathcal{B}_4$.

When factors $\mathcal{A}$ and $\mathcal{B}$ are at levels of $\mathcal{A}_i$ and $\mathcal{B}_j$, τ_{gfr} can be regarded as τ_{gfr}^{ij}, and $\tau_{\mathrm{gfr}}^{ij} \sim \mathcal{N}(\mu_{\tau_{\mathrm{gfr}}^{ij}}, \sigma^2_{\tau_{\mathrm{gfr}}})$. In the following, τ_{gfr}^{ij} is written as X_{ij} for convenience.

Let

$$\begin{cases} \mathrm{SS}_{\mathcal{A}} = bm\sum_{i=1}^{a}(\bar{X}_{i..} - \bar{X})^2 \\ \mathrm{SS}_{\mathcal{B}} = \mathrm{gfr}\sum_{j=1}^{b}(\bar{X}_{.j.} - \bar{X})^2 \\ \mathrm{SS}_{\mathcal{A}\times\mathcal{B}} = m\sum_{i=1}^{a}\sum_{j=1}^{b}(\bar{X}_{ij.} - \bar{X}_{i..} - \bar{X}_{.j.} + \bar{X})^2 \\ \mathrm{SS}_{\mathrm{e}} = \sum_{i=1}^{a}\sum_{j=1}^{b}\sum_{k=1}^{m}(X_{ijk} - \bar{X}_{ij.})^2 \end{cases} \tag{17}$$

where

$$\begin{cases} \bar{X}_{ij.} = \dfrac{1}{m}\sum_{k=1}^{m}X_{ijk} \qquad i = 1, 2, \cdots, 6;\ j = 1, 2, 3, 4 \\ \bar{X}_{i..} = \dfrac{1}{bm}\sum_{j=1}^{a}\sum_{k=1}^{m}X_{ijk} = \dfrac{1}{b}\sum_{j=1}^{b}\bar{X}_{ij.} \qquad i = 1, 2, \cdots, 6; \\ \bar{X}_{.j.} = \dfrac{1}{gfr}\sum_{i=1}^{a}\sum_{k=1}^{m}X_{ijk} = \dfrac{1}{a}\sum_{i=1}^{a}\bar{X}_{ij.} \qquad j = 1, 2, 3, 4 \\ \bar{X} = \dfrac{1}{abm}\sum_{i=1}^{a}\sum_{j=1}^{b}\sum_{k=1}^{m}X_{ijk} = \dfrac{1}{ab}\sum_{i=1}^{a}\sum_{j=1}^{a}X_{ij.} = \dfrac{1}{a}\sum_{i=1}^{a}\bar{X}_{i..} \\ \quad = \dfrac{1}{b}\sum_{j=1}^{b}\bar{X}_{.j.} \end{cases}$$

In Eq. (17), $\mathrm{SS}_{\mathcal{A}}$, $\mathrm{SS}_{\mathcal{B}}$ and $\mathrm{SS}_{\mathcal{A}\times\mathcal{B}}$ are defined as the sum of squares for $\mathcal{A}$, $\mathcal{B}$ and $\mathcal{A}\times\mathcal{B}$, respectively. In addition, SS_{e} is defined as the sum of squares of the errors; a and b are levels of $\mathcal{A}$ and $\mathcal{B}$, respectively; m, $\sum$ and $\mathcal{A}\times\mathcal{B}$ are sum of every test state, summation operator and interaction of $\mathcal{A}$ and $\mathcal{B}$ on X_{ij}, respectively.

Let $n = abm$.

According to the theory of mathematical statistics [27], because $X_{ijk} \sim \mathcal{N}(\mu_X, \sigma_X^2)$, the statistical variables, $\mathrm{SS}_{\mathcal{A}}$, $\mathrm{SS}_{\mathcal{B}}$, $\mathrm{SS}_{\mathcal{A}\times\mathcal{B}}$ and SS_{e}, are independent of one another, and the statistical variable $(\mathrm{SS}_{\mathrm{e}}/\sigma_X^2)$ has a $\chi^2(n-ab)$ distribution. Furthermore, if factors $\mathcal{A}$, $\mathcal{B}$ and $\mathcal{A}\times\mathcal{B}$ have no effect on the test data X_{ijk}, the statistical variables, $(\mathrm{SS}_{\mathcal{A}}/\sigma_X^2)$, $(\mathrm{SS}_{\mathcal{B}}/\sigma_X^2)$ and $(\mathrm{SS}_{\mathcal{A}\times\mathcal{B}}/\sigma_X^2)$ have a $\chi^2(a-1)$ distribution, $\chi^2(b-1)$ distribution and $\chi^2((a-1)(b-1))$ distribution, respectively. Furthermore, $(\mathrm{SS}_{\mathcal{A}}/\mathrm{SS}_{\mathrm{e}})$, $(\mathrm{SS}_{\mathcal{B}}/\mathrm{SS}_{\mathrm{e}})$ and $(\mathrm{SS}_{\mathcal{A}\times\mathcal{B}}/\mathrm{SS}_{\mathrm{e}})$ have a $\mathcal{F}(a-1, n-ab)$ distribution, $\mathcal{F}(b-1, n-ab)$ distribution and $\mathcal{F}((a-1)(b-1), n-ab)$ distribution, respectively.

By analyzing the data in Table 2 with the methodology of variance analysis, we obtain the result listed in Table 3, and conclusions as follows:

According to the definition of the $\mathcal{F}$distribution, the critical theory values of $\mathcal{F}_{0.95}(5, 24)$, $\mathcal{F}_{0.95}(3, 24)$ and $\mathcal{F}_{0.95}(15, 25)$ are 2.62, 3.01 and 2.11, respectively.

The values of $\mathcal{F}$ in Table 3 are greater than the critical theory values of $\mathcal{F}_{0.95}(5, 24)$, $\mathcal{F}_{0.95}(3, 24)$ and $\mathcal{F}_{0.95}(15, 25)$. Therefore, the assumption that factors $\mathcal{A}$, $\mathcal{A}$ and $\mathcal{A}\times\mathcal{B}$ have no effect on X_{ij} turns out to be false. This result explains the time-varying and nonlinear property of τ_{gfr}. Furthermore, by comparing differences between the three values of $\mathcal{F}$ in Table 3 and their corresponding critical theory values, $\mathcal{F}_{0.95}(5, 24)$, $\mathcal{F}_{0.95}(3, 24)$ and $\mathcal{F}_{0.95}(15, 25)$, it is obvious the difference of factor $\mathcal{A}$ with its critical theory value stands out. This is because factor $\mathcal{A}$ has a greater effect on τ_{gfr}.

3. Adaptive control strategy of airflow

To optimize the operating performance of the air-supply subsystem, adaptive control is employed to alleviate the dynamic variation arising from the time-varying property at different operating points. This strategy, illustrated in Fig. 7, includes on-line parameter identification and real-time assignment of the closed-loop poles according to the identified results.

In the process of operation, four goals are to be achieved: (1) to quantify the desired airflow; (2) to define the ideal kinetics of air replenishment into the cathode; (3) to design a controller, under the regulation of which, airflow responds to the reference command dynamically and accurately; (4) to estimate time-varying parameters in real time, modify dynamics of the air-supply closed-loop subsystem and consequently ensure the airflow approaches the desired airflow with a certain precision.

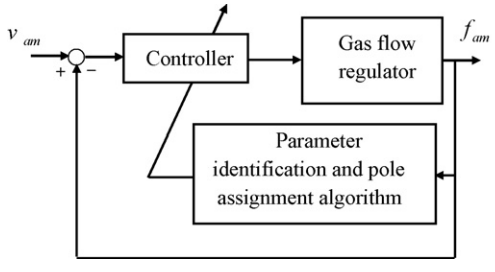

Fig. 7. Adaptive controller.

Table 3
Variance analysis result of τ_{gfr}

Source of variance	Sum of squares	Degree of freedom	Sum of mean squares	Value of F
$\mathcal{A}$	7.4914	5	1.4983	123.5155
$\mathcal{B}$	2.8194	3	0.1226	10.1056
$\mathcal{A} \times \mathcal{B}$	0.5957	15	0.0397	3.2738
Error	0.2911	24	0	

3.1. Airflow supply

As airflow is directly related to the output power of a fuel cell system, much attention has been devoted to airflow replenishment. Gelfi et al. [28] compared dynamic flow capabilities of a compressor of a fuel cell system with a blower. The paper showed the two systems were dynamically similar in providing airflow in the cathode channel. The blower spent time spinning its rotor inertia, whereas the compressor spent time pushing air and elevating supply manifold pressure. Suh and Stefanopoulou [29] surveyed the dynamic coupling between a compressor and a fuel cell system when the compressor motor was driven by the stack power.

For several reasons [9,30], the airflow supplied to the cathode should exceed the airflow necessary for reaction. This leads to an oxygen excess ratio, λ_{O_2}, which is defined as the ratio of oxygen supplied to oxygen used in the cathode. A high oxygen excess ratio, and thus a high oxygen partial pressure, improves the output power of a fuel cell stack. However, after an optimum value of the oxygen excess ratio is reached, any further increase will cause an excessive increase in compressor power and thus deteriorate the system's net power. Pukruspan [12], in his doctorate thesis, showed by experiment that the highest net power was achieved at an oxygen excess ratio between 2 and 2.4 depending on the stack current in the fuel cell system, whereas experimental data [31] showed the optimum oxygen excess ratio of our fuel cell system is $\lambda_{O_2} = 1.5$. Therefore the expected airflow in this paper is

$$f_{air,ca,ex} = \lambda_{O_2} \frac{Ni_{st}}{0.21 \times 4F} \tag{18}$$

3.2. Desired kinetics of the air-supply subsystem

After considering a variety of factors, the optimum dynamics of our air-supply subsystem is

$$\begin{cases} \tau_{gfr,m} \dfrac{df_{air,gfr}}{dt} = -f_{air,gfr} + k_{wf} K_{gfr} u_{gfr} \\ u_{gfr} = \dfrac{f_{air,ca,ex}}{k_{wf} K_{gfr}} \end{cases} \tag{19}$$

where $\tau_{gfr,m}$ is the optimum time constant of the airflow meter.

The corresponding discrete-time model of Eq. (19) is

$$f_{air,gfr}(k) = b_{gfr,m} \frac{1 + q^{-1}}{1 + a_{gfr,m} q^{-1}} f_{air,gfr,ex}(k) \tag{20}$$

where $b_{gfr,m} = \tau_s/(\tau_s + 2\tau_{gfr,m})$, $a_{gfr} = (\tau_s - 2\tau_{gfr,m})/(\tau_s + 2\tau_{gfr,m})$

3.3. Controller design

To facilitate the design of digital controller, the model of the gas flow regulator Eq. (9) is represented as a discrete-time equation of the difference operator as

$$\begin{aligned}(1 + a_{air} q^{-1}) f_{air,gfr} = {} & b_{air}(1 + q^{-1}) k_{wf} K_{gfr} u_{gfr}(k) \\ & + b_{air}(1 + q^{-1}) \epsilon(k)\end{aligned} \tag{21}$$

where $b_{gfr} = \tau_s/(\tau_s + 2\tau_{gfr})$, $a_{gfr} = (\tau_s - 2\tau_{gfr})/(\tau_s + 2\tau_{gfr})$; and τ_s is the sample time.

To ensure the airflow dynamically tracks the reference command with a certain precision at a particular operating point, a control strategy is employed to assign poles of the air-supply subsystem for which the time-varying parameter is identified on-line,[3] and eventually, the dynamics of the air-supply subsystem approach the described by Eq. (19). To achieve this goal, the following control method is adopted:

$$\begin{aligned} W_{gfr}(q^{-1}) k_{wf} K_{gfr} u_{gfr}(k) = {} & H_{gfr}(q^{-1}) f_{air,gfr,ex}(k) \\ & - G_{gfr}(q^{-1}) f_{air,gfr}(k) \end{aligned} \tag{22}$$

where, $H_{gfr}(q^{-1}) = (b_{gfr,m}/b_{am})$. $W_{am}(q^{-1})$ and $G_{am}(q^{-1})$ can be solved according to the following Diophantine equation:

$$A_{gfr}(q^{-1}) W_{gfr}(q^{-1}) + B_{gfr}(q^{-1}) G_{gfr}(q^{-1}) = A_{gfr,m}(q^{-1}) \tag{23}$$

where

$$\begin{cases} A_{gfr}(q^{-1}) = 1 + a_{gfr} q^{-1} \\ B_{gfr}(q^{-1}) = b_{gfr} + b_{gfr} q^{-1} \\ C_{gfr}(q^{-1}) = c_{gfr} + c_{gfr} q^{-1} \\ A_{gfr,m}(q^{-1}) = 1 + a_{gfr,m} q^{-1} \\ B_{gfr,m}(q^{-1}) = H_{gfr}(q^{-1}) B_{gfr}(q^{-1}) \\ W_{gfr}(q^{-1}) = w_{gfr} \\ G_{gfr}(q^{-1}) = g_{gfr} \end{cases}$$

Solving the Diophantine equation, we get

$$\begin{cases} W_{gfr}(q^{-1}) = \dfrac{1 - a_{gfr,m}}{1 - a_{gfr}} \\ G_{gfr}(q^{-1}) = \dfrac{a_{gfr,m} - a_{gfr}}{b_{gfr}(1 - a_{gfr})} \end{cases} \tag{24}$$

[3] The method for closed-loop parameter identification will be presented in the following subsection.

Substituting $W_{gfr}(q^{-1})$, $G_{gfr}(q^{-1})$ and $H_{gfr}(q^{-1})$ into Eq. (22), the control command can be obtained as

$$u_{gfr}(k) = \frac{1}{k_{wf}K_{gfr}b_{air}(1-a_{air,m})}[b_{air,m}(1-a_{air})f_{air,gfr,ex}(k) - (a_{air,m}-a_{air})f_{air,gfr}(k)] \quad (25)$$

Furthermore, the closed-loop dynamics of the air-supply subsystem could be deduced in joint consideration of Eq. (21) and the control command as

$$f_{air,ca}(k) = \frac{b_{air,m}(1+q^{-1})}{1+a_{air,m}q^{-1}}f_{air,gfr,ex}(k) + b_{air}\frac{1-a_{air,m}}{1-a_{air}}\frac{1+a_{air}q^{-1}}{1+a_{air,m}q^{-1}}\epsilon(k) \quad (26)$$

3.4. Closed-loop parameter identification

Variation of the main time constant of the gas flow regulator mainly arising from its time-varying property, often occurs with the shift of the operating point in the air-supply subsystem. This directly leads to a discrepancy between the real airflow dynamics and its desired counterpart. To reduce the influence of the variation, on-line modification of dynamics of the air-supply subsystem is necessary. The premise this application is the identification of the main time constant in the closed-loop air-supply subsystem. As is well known, parameter identification in a closed-loop system is more difficult than that in an open-loop system, and in most cases, this task is unrealizable. Next, we will prove, in theory, that time-varying parameters in an gas flow regulator are identifiable in the closed-loop air-supply subsystem.

Proof. Considering the model of the air-supply, i.e. Eq. (21) and its control equation Eq. (22), the closed-loop subsystem can be expressed as

$$(A_{gfr}(q^{-1})W_{gfr}(q^{-1}) + B_{gfr}(q^{-1})G_{gfr}(q^{-1}))f_{air,gfr}(k) = H_{gfr}(q^{-1})B_{gfr}(q^{-1})f_{air,gfr,ex}(k) + C_{gfr}(q^{-1})W_{gfr}(q^{-1})\epsilon(k) \quad (27)$$

where

$$\begin{cases} \deg W_{gfr}(q^{-1}) = 0 \\ \deg G_{gfr}(q^{-1}) = 0 \\ \deg H_{gfr}(q^{-1}) = 0 \end{cases} \quad (28)$$

Let

$$P_{gfr} = -H_{gfr}(q^{-1})B_{gfr}(q^{-1})f_{air,gfr,ex}(k) + (B_{gfr}(q^{-1})G_{gfr}(q^{-1}) + A_{gfr}(q^{-1})W_{gfr}(q^{-1}))f_{air,gfr}(k) \quad (29)$$

then Eq. (27) can be reformed as

$$P_{gfr} = W_{gfr}C_{gfr}\epsilon(k) \quad (30)$$

where

$$\begin{cases} P_{gfr} = p_{gfr,0} + p_{gfr,1}q^{-1} \\ p_{gfr,0} = f_{air,gfr}(k) - b_{gfr}f_{air,gfr,ex}(k) \\ p_{gfr,1} = a_{gfr}f_{air,gfr}(k) - b_{gfr}f_{air,gfr,ex}(k) \end{cases} \quad (31)$$

According to the principle of parameter identification, if P_{gfr} and C_{gfr} are prime to each other, elements of P_{gfr}, $p_{gfr,0}$ and $p_{gfr,1}$ are identifiable as $\epsilon(k)$ belongs to Gaussian distribution. As the only factor of C_{gfr} is $(1+q^{-1})$, to prove P_{am} and C_{am} are prime to each other is to prove there is no $(1+q^{-1})$ in P_{gfr}. As $\deg A_{gfr}(q^{-1}) = 1$, if $p_{gfr,0} \neq p_{am,1}$, it can be concluded there is no $(1+q^{-1})$ in P_{am}.

Because

$$p_{gfr,1} - p_{gfr,0} = (a_{gfr}-1)f_{air,gfr}(k) \quad (32)$$

it is easy to conclude that, if $a_{gfr} \neq 1$, then $p_{gfr,0} \neq p_{gfr,1}$. Due to $a_{gfr} = (\tau_s - 2\tau_{gfr})/(\tau_s + 2\tau_{gfr})$, it is obvious that the inequality of $a_{gfr} \neq 1$ comes into existence, namely, $p_{am,0} \neq p_{am,1}$. It can be deduced the elements P_{am} and C_{am} are prime to each other. So far, conclusion can be deduced that the elements of P_{am}, namely $p_{am,0}$ and $p_{am,1}$ are identifiable.

Assuming that a certain method, such as least squares identification or maximum likelihood estimation, is applied to identify $p_{gfr,0}$ and $p_{gfr,1}$, the results are $\hat{p}_{gfr,0}$ and $\hat{p}_{gfr,1}$, respectively.

In addition, because $b_{gfr} = \tau_s/(2\tau_{am} + \tau_s)$ and $a_{am} = (\tau_s - 2\tau_{am})/(\tau_s + 2\tau_{am})$, it is clear that b_{am} and a_{am} are dependent on each other, and their relationship can be expressed as

$$2b_{gfr} = a_{gfr} + 1 \quad (33)$$

Applying $\hat{p}_{gfr,0}$, $\hat{p}_{gfr,1}$, $H_{gfr}(q^{-1}) = (b_{gfr,m}/b_{gfr})$, $2b_{am} = a_{am} + 1$ and substituting Eq. (24) into Eq. (29), we can get

$$M\begin{pmatrix} a_{gfr}^2 \\ a_{gfr} \end{pmatrix} = \begin{pmatrix} \hat{p}_{gfr,0} - f_{air,gfr}(k)(1+a_{gfr,m}) \\ +b_{gfr,m}f_{air,gfr,ex}(k) \\ \hat{p}_{gfr,1} - 2a_{gfr,m}f_{air,gfr}(k) \\ +b_{gfr,m}f_{air,ca,ex}(k) \end{pmatrix} \quad (34)$$

where

$$M = \begin{pmatrix} b_{gfr,f}f_{air,gfr,ex}(k) - 2f_{air,gfr}(k) + \hat{p}_{gfr,0} & (a_{gfr,m}-1)f_{air,gfr}(k) \\ b_{gfr,m}f_{air,ca,ex}(k) - f_{air,gfr}(k) - a_{gfr,m}f_{air,gfr}(k) + \hat{p}_{gfr,1} & (a_{gfr,m}-1)f_{air,gfr}(k) \end{pmatrix}$$

and

$$\det(M) = \hat{p}_{gfr,1} - \hat{p}_{gfr,0} - (a_{gfr,m}-1)f_{air,gfr}(k) \quad (35)$$

where $\det(M)$ is the determinant of the square matrix M.

According to Eq. (32), if the dynamics of the air-supply subsystem converge to Eq. (20), the determinant of M converges to zero. This means the two equations in Eq. (34) are linearly dependent on one another, and the estimation of a_{gfr} can be obtained by solving either of them. At the same time, an estimation of b_{gfr} can be inferred from Eq. (33).

Next, least squares identification is discussed to estimate a_{gfr} and b_{gfr} in the air-supply closed-loop system.

It is easy to rearrange Eq. (21) into an ideal form for least squares identification as

$$f_{air,gfr}(k) = h^T\theta + b_{gfr}w_{gfr}(\epsilon(k) + \epsilon(k-1)) \tag{36}$$

where

$$\begin{cases} h = [0.5k_{wf}K_{gfr}(u_{gfr}(k) + u_{gfr}(k-1)) \\ \quad -f_{air,gfr}(k-1), 0.5k_{wf}K_{gfr}(u_{gfr}(k) + u_{gfr}(k-1))]^T \\ \theta = [a_{gfr}, 1]^T \end{cases}$$

In addition, in the air-supply subsystem, $f_{air,gfr}$ can be measured directly by the flow meter built in gas flow regulator.

A recursion algorithm can be expressed as

$$\begin{cases} P_{gfr}(0) = \alpha_{gfr}^2 I_{2\times 2} \\ \hat{\theta}(0) = \beta_{gfr}\hat{\theta}(k+1) = K_{gfr}(k+1)[u_0(k+1) \\ \quad +\hat{\theta}(k) - h_{gfr}^T(k+1)\hat{\theta}(k)] \\ K_{gfr}(k+1) = [h_{gfr}^T(k+1)P_{gfr}h_{gfr}(k+1) \\ \quad +\mu_{gfr}]^{-1}P_{gfr}(k)h_{gfr}(k+1) \\ P_{gfr}(k+1) = \dfrac{1}{\mu_{gfr}}[I - K_{gfr}(k+1)h_{gfr}^T(k+1)]P_{gfr}(k) \\ 0 < \mu_{gfr} < 1 \end{cases} \tag{37}$$

where α_{gfr} is a sufficiently large real number, and β_{gfr} is a sufficiently small 2×1 dimensional vector.

According to Eq. (33), the estimation of b_{gfr} could be deduced as

$$\hat{b}_{gfr} = \frac{\hat{a}_{gfr} + 1}{2} \tag{38}$$

In the air-supply subsystem, it is practical to estimate the parameters of $\hat{a}_{gfr}$ and $\hat{b}_{gfr}$ by least squares identification and subsequently to modify the kinetics of the closed-loop air-supply subsystem. This method is the so-called adaptive strategy for air replenishment control of the air-supply subsystem. The step-by-step procedure for this strategy is expressed:

(1) Initialize $\hat{a}_{gfr}(0)$.
(2) Get w_{gfr}, g_{gfr} and h_{gfr} by solving Eq. (23).
(3) Determine $f_{air,gfr}$ by solving Eq. (22) and subsequently apply it to the air-supply system.
(4) Save $f_{air,gfr}(k-1)$ and sample $f_{air,gfr}(k)$, and at the same time determine the reference command $u_{gfr}(k)$.
(5) With $f_{air,gfr}(k-1)$, $f_{air,gfr}(k)$ and u_{gfr}, estimate $a_{gfr}(k)$ and $b_{gfr}(k)$ by least squares identification.
(6) Return to step (2).

4. Test and experiment

The fuel cell test bench in this paper was designed and assembled by CASIA (Institute of Automation, Chinese Academy of Sciences). This test bench, as shown in Fig. 8, mainly includes the fuel cell system described above, a dc/dc converter for stack voltage stabilization (dc/dc output voltage of 12 V), a current regulator for stack current control, a battery as auxiliary power, a regulatable resistor as a load with maximum power of 800 W and a electric motorcycle with maximum power of 500 W. To verify the control strategy described above, a test comparison is made under the control strategy of the pole assignment described in Section 3.3 with and without τ_{gfr} identification. In the former case, the ideal value of τ_{gfr} is set at 2.3 s, and in the latter case, the value of τ_{gfr} varies according to the shift of the operating point.

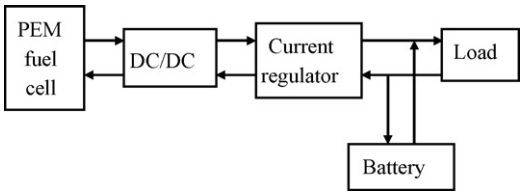

Fig. 8. Scheme of test bench.

In tests, operating points of the fuel cell system are regulated through changes of airflow in the gas flow regulator and of stack current.

(1) Test 1

The stack current is regulated to reach 40 A by coordination of the current regulator and the resistor, and the cathode pressure is controlled at 30 kPa (relative to atmospheric pressure). There are two airflow operating points at 0.00176 and 0.00238 mol s^{-1}. Step disturbances of airflow at 0.0002 mol s^{-1} are exerted on the gas flow regulator as reference command changes at these two operating points.

Test data are shown in Figs. 9 and 10. Theoretically, the time span for the step response of a first order linear system to reach 61.9% of the stable output altitude is the system's time constant. The dotted lines in Figs. 9 and 10 represent 61.9% of the stable output airflow, and thus, the abscissa of the intersection point between the dotted line and test data (solid line) is equal to the time constant of the gas flow regulator.

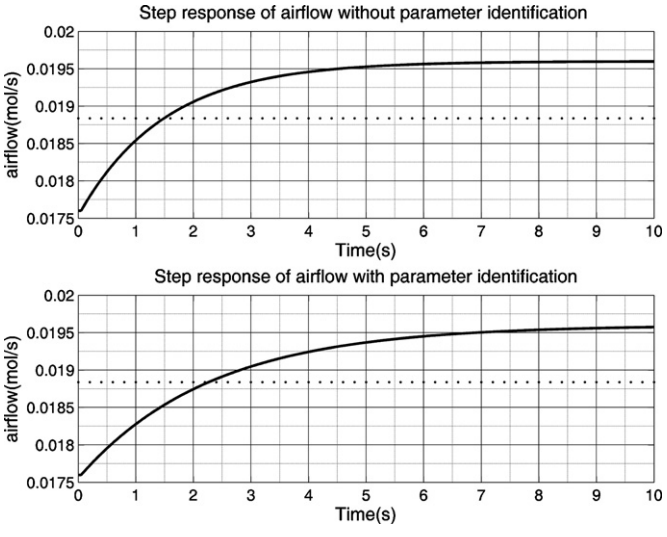

Fig. 9. Test data at the operating point of $f_{ari,gfr} = 0.0176$ mol s^{-1}.

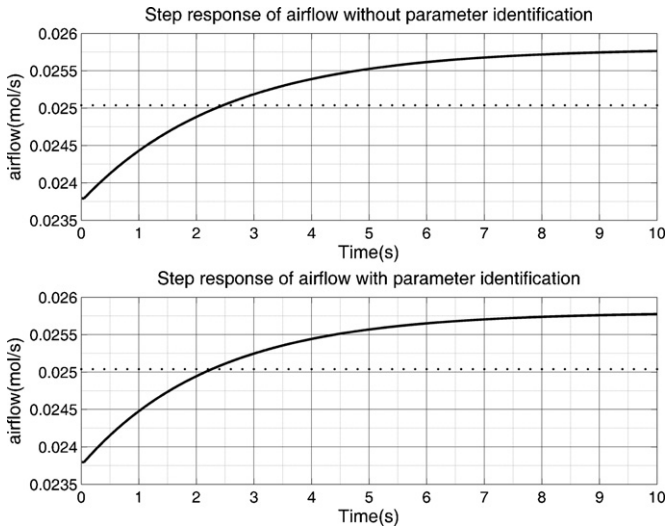

Fig. 10. Test data at the operating point of $f_{\text{ari,gfr}} = 0.0238\,\text{mol}\,\text{s}^{-1}$.

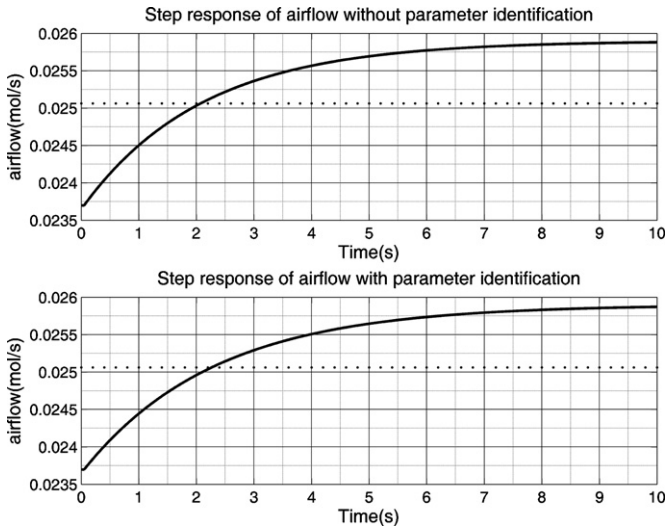

Fig. 12. Test data at the operating point of $i_{\text{st}} = 40\,\text{A}$.

It is easy to see the time constants in the system with parameter identification at the two operating points are almost equal at 2.3 s. However, the time constants in the system without parameter identification vary obviously from 1.5 to 2.4 s.

(2) Test 2

The OTPV is fixed at a suitable position and the stack current operating points are fixed at 30 and 40 A with corresponding airflows of 0.00133 and 0.00237 mol s^{-1}. Step disturbance of the stack current is 5 A at these operating points. The controller can adjust airflow to track the step disturbance of the stack current with an oxygen excess ratio of 1.5. The dynamics of the gas flow regulator are compared for these closed-loop air-supply subsystems.

According to the test data in Figs. 11 and 12, it is obvious the time constants in the system with parameter identification at the two operating points are almost equal at 2.3 s. However, time constants in the system without parameter identification vary obviously from 1.77 to 2.1 s.

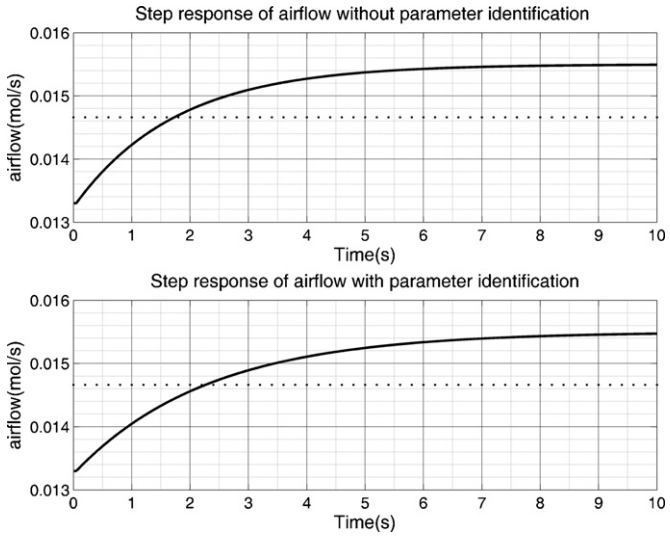

Fig. 11. Test data at the operating point of $i_{\text{st}} = 30\,\text{A}$.

(3) Test 3

The motorcycle is connected to the current regulator as load and the initial power of the cycle is controlled at about 120 W which responds to stack current at about 9 A. Abrupt acceleration is performed through regulation of the accelerograph. Stack current change to 15.5 A in the adaptive controller case and 15 A in the non-adaptive controller case, respectively. Test data in Fig. 13 shows the time constant is about 2.3 s, i.e. the ideal value, in the adaptive controller case, while the time constant is about 1.8 s in non-adaptive controller case which obviously departs from the ideal one. From the test results in Figs. 9–13, it can be concluded adoption of the adaptive control strategy can be used to adjust the gas flow regulator time constant to a fixed point, and consequently make the gas flow regulator perform with an desired dynamic action.

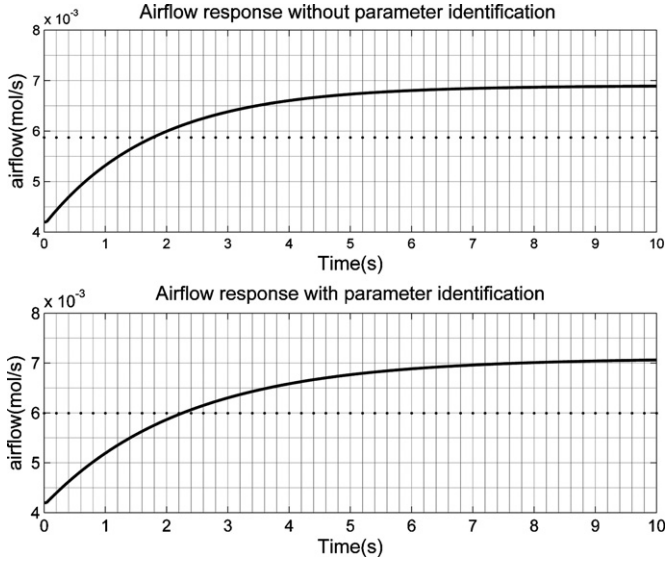

Fig. 13. Test data in motorcycle case.

5. Conclusion

Technically, PEM fuel cell systems could become viable propulsion system alternatives to conventional combustion engines, as long as a sufficient amount of power output is available to meet the need of the load. To achieve this goal, every subsystem of a fuel cell system has to act smoothly and be dynamically co-operative with each other. However, the time-varying and nonlinear characteristics of these subsystems are obstacles during operation. To run the air-supply subsystem to meet the need of air replenishment into the cathode, this paper proposes an adaptive control strategy to regulate the dynamics of the subsystem at different operating points. A summary of new findings obtained is as

(1) Experimentally find the time-varying and nonlinear properties of the gas flow regulator.
(2) Optimize the kinetics of the air-supply subsystem by designing an algorithm for pole reassignment via the solution of a Diophantine equation.
(3) Theoretically find the the time-varying parameter of the gas flow regulator identifiable in the closed-loop system, and subsequently apply the least squares identification algorithm to estimate the time-varying parameter and eventually propose an adaptive strategy for the control of the air-supply subsystem.
(4) Compare the control strategy with and without parameter identification, and verify the validity of the adaptive strategy.

The tests have shown the designed adaptive control strategy can lead to good system performance and stability. Although this paper is limited to the control of the air-supply subsystem only, it is important to note the adaptive principles can be easily applied to other subsystems of the fuel cell system.

Further work will include: (1) examination of the influence of cathode pressure on airflow, (2) investigation of the stack current impact on the kinetics of air replenishment into the cathode and (3) integration of an air-supply subsystem with other subsystems into an organic unity.

Acknowledgments

Financial support by the National High Technology Research Plan of China (863Plan) under contracts 2006AA11A102 and Laboratory of Complex Systems and Intelligence Science, Institute of Automation, Chinese Academy of Sciences, PR China, (CASIA) is gratefully appreciated. Many thanks go to professor Guoping Liu (CASIA) for his help and controller implementation for the fuel cell testbench and also to Yingfei Xiong (CASIA), Xianrui Deng (CASIA), and Shiwen Tong (CASIA), for all the helpful discussions.

References

[1] S. Srinivasan, D.J. Manko, H. Koch, M.A. Enayetullah, J.A. Appleby, Journal of Power Sources 29 (1990) 367–387.
[2] V. Mehta, J.S. Cooper, Journal of Power Sources 114 (2003) 32–53.
[3] A.F. Ghenciu, Current Opinion in Solid State and Materials Science 6 (2002) 389–399.
[4] P. Costamagna, S. Srinivasan, Journal of Power Sources 102 (2001) 242–252.
[5] J.M. Cunningham, D.J. Friedman, M.A. Hoffman, R.M. Moore, Requirements for a Flexible and Realistic Air Supply Model for Incorporation into a Fuel Cell Vehicle (FCV) System Simulation, SAE paper 1999-01-2912 in SP-1466, 1999, pp. 43–48.
[6] Z.X. Liu, L.Z. Yang, Z.Q. Mao, W.L. Zhuge, Y.J. Zhang, L.S. Wang, Journal of Power Sources 157 (2006) 166–176.
[7] S.D. Knights, K.M. Colbow, J.S. Pierre, D.P. Wilkinson, Journal of Power Sources 127 (2004) 127–134.
[8] T.R. Ralph, M.P. Hogarth, Platinum Metals Review (UK) 46 (2002) 117–135.
[9] J.T. Pukrushpan, A.G. Stefanopoulou, H. Peng, Control of Fuel Cell Power Systems: Principles, Modelling, Analysis and Feedback Design, Spriger, Berlin, 2004.
[10] S. Kim, S. Shimpalee, J.W. Van Zee, Journal of Power Sources 137 (2004) 43–52.
[11] A. Vahidi, A. Stefanopoulou, H. Peng, pp. 834–839 Proceddings of the American Control Conference, vol. 1, 2004.
[12] J.T. Pukrushpan, Modeling and Control of Fuel Cell Systems and Fuel Processors, The University of Michigan, 2003.
[13] R.N. Methekar, V. Prasad, R.D. Gudi, Journal of Power Sources 165 (2007) 152–170.
[14] D. Feroldi, M. Serra, J. Riera, Journal of Power Sources 76 (2007) 205–212.
[15] P. Rodatz, G. Paganelli, L. Guzzella, Proceedings of the American Control Conference, Adams Mark Hotel, Denver, CO, June 4–6, 2003, pp. 2043–2048.
[16] J.T. Pukrushpan, A.G. Stefanopoulou, H. Peng, Proceedings of the American Control Conference, Anchorage, Alaska, May 8–10, 2002.
[17] J.T. Pukrushpan, A.G. Stefanopoulou, H. Peng, IEEE Control System Magazine 24 (2004) 30–46.
[18] S. Caux, J. Lachzize, M. Fadel, P. Schott, L. Nicod, Proceedings of the 2005 IEEE Vehicle Power and Propulsion (VPP) Conference, Illinois Institute of Technology, Chicago, Illinois, USA, September 7–9, 2005, pp. 597–602.
[19] Y.P. Yang, F.C. Wang, H.P. Chang, Y.W. Ma, B.J. Weng, Journal of Power Sources 164 (2007) 761–771.
[20] J. Golbert, D.R. Lewin, Journal of Power Sources 135 (2004) 135–151.
[21] J.A. Adams, W.C. Yang, K.A. Oglesby, K.D. Osborne, The development of Ford's P2000 fuel cell vehicle, SAE Paper, 2000–01-1061.
[22] P. Sridhar, R. Perumal, N. Rajalakshmi, M. Raja, K.S. Dhathathreyan, Journal of Power Sources 101 (2001) 72–78.
[23] C.Y. Chow, B.M. Wozniczka, Electrochemical fuel cell stack with humidification section located upstream from the electrochemically active section, U.S. Patent No. 5,382,478 (1995).
[24] X.R. Deng, Modeling and Control of the Thermal and Humidification Systems of a PEM Fuel Cell, Dissertation for Doctor Degree, Institute of Automation, Chinese Academy of Sciences, 2006.
[25] G.D. Liu, Research of the Electric Energy Systems of a PEM Fuel Cell, Dissertation for Doctor Degree, Institute of Automation, Chinese Academy of Sciences, 2007.
[26] G.C. Goodwin, K.S. Sin, Adaptive filtering Prediction and Control, Prentice-Hall, Englewood Cliffs, NJ, 1984.
[27] V.K. Rohatgi, An Introduction to Probaility Theory and Mathematical Statistics, John Wiley & Sons, 1976.
[28] S. Gelfi, A.G. Stefanopoulou, J.T. Pukruspan, H. Peng, Proceedings of the 2003 American Control Conference, vol. 3, Denver, CO, 2003, pp. 2049–2054.
[29] K.W. Suh, A.G. Stefanopoulou, International Journal of Energy Research 29 (2005) 1167–1189.
[30] G. Boehm, D.P. Wilkinson, S. Khight, R. Schamm, N.J. Fletcher, Method and apparatus for operating a fuel cell, United States Patent No. 6,461,751 (2002).
[31] Y.F. Xiong, Modeling and Control of a Small PEM Fuel Cell Flow System, Dissertation for Doctor Degree, Institute of Automation, Chinese Academy of Sciences, 2006.